IOP PUBLISHING PHYSICAL BIOLOGY
Phys. Biol. **9** (2012) 000000 (10pp) UNCORRECTED PROOF

Optimal cellular mobility for synchronization arising from the gradual recovery of intercellular interactions

Koichiro Uriu[1,2,3,6], **Saúl Ares**[3,4,7], **Andrew C Oates**[2] **and Luis G Morelli**[2,3,5,6]

[1] Theoretical Biology Laboratory, RIKEN Advanced Science Institute, 2-1 Hirosawa, Wako, Saitama, 351-0198, Japan
[2] Max Planck Institute of Molecular Cell Biology and Genetics, Pfotenhauerstr. 108, 01307 Dresden, Germany
[3] Max Planck Institute for the Physics of Complex Systems, Nöthnitzer Str. 38, 01187 Dresden, Germany
[4] Grupo Interdisciplinar de Sistemas Complejos (GISC), Madrid, Spain
[5] Departamento de Fisica, FCEyN, UBA, Ciudad Universitaria, 1428 Buenos Aires, Argentina

E-mail: uriu@mpi-cbg.de and morelli@mpi-cbg.de

Received 7 March 2012
Accepted for publication 5 April 2012
Published DD MM 2012
Online at stacks.iop.org/PhysBio/9/000000

Abstract
Cell movement and intercellular signaling occur simultaneously during the development of tissues, but little is known about how movement affects signaling. Previous theoretical studies have shown that faster moving cells favor synchronization across a population of locally coupled genetic oscillators. An important assumption in these studies is that cells can immediately interact with their new neighbors after arriving at a new location. However, intercellular interactions in cellular systems may need some time to become fully established. How movement affects synchronization in this situation has not been examined. Here, we develop a coupled phase oscillator model in which we consider cell movement and the gradual recovery of intercellular coupling experienced by a cell after movement, characterized by a moving rate and a coupling recovery rate, respectively. We find (1) an optimal moving rate for synchronization and (2) a critical moving rate above which achieving synchronization is not possible. These results indicate that the extent to which movement enhances synchrony is limited by a gradual recovery of coupling. These findings suggest that the ratio of time scales of movement and signaling recovery is critical for information transfer between moving cells.

S Online supplementary data available from stacks.iop.org/PhysBio/9/000000/mmedia

Q1 (Some figures may appear in colour only in the online journal)

1. Introduction

Intercellular communication via direct cell–cell contact allows the flow of information in tissues during development. Information is exchanged between cells using a diverse set of ligands and receptors expressed on the cells' surfaces, including but not limited to Eph–ephrin, Cadherin–Cadherin and Delta–Notch receptor–ligand pairs [1–3]. This information is used to coordinate the dynamics of cellular processes across tissues and establish patterns. During development, cellular movement can occur within tissues as they undergo morphogenesis [4, 5]. Our interest is how these cellular movements affect the emergence of organized spatial and temporal patterns that yield a reliable developmental program.

[6] Authors to whom any correspondence should be addressed.
[7] Present address: Logic of Genomic Systems Laboratory, Centro Nacional de Biotecnología—CSIC, Calle Darwin 3, 28049 Madrid, Spain.

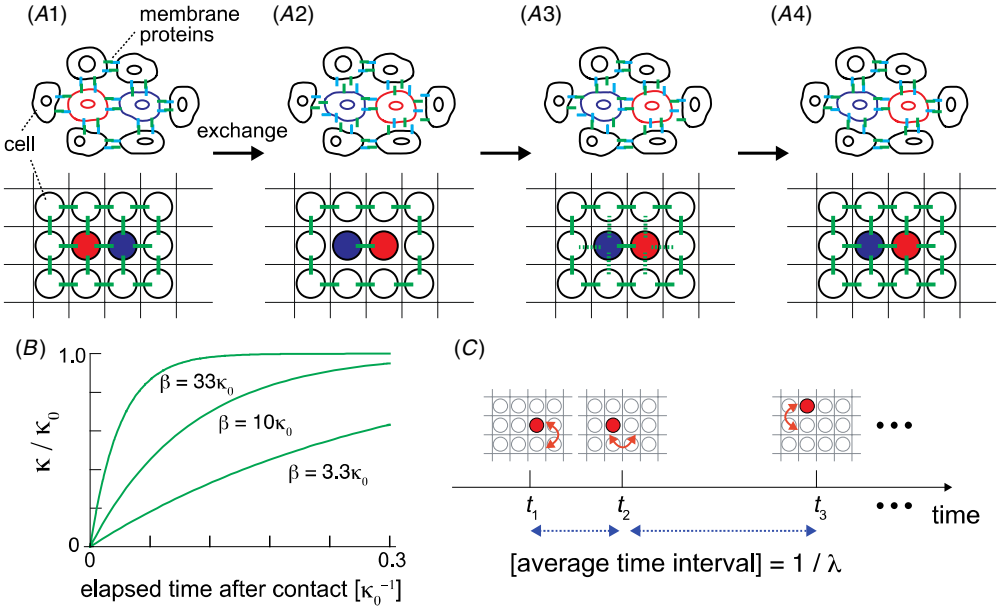

Figure 1. Cells need to recover interactions with their new neighbors after movement. (*A*1) Cells in a two-dimensional lattice. Two cells connected with a solid green line can interact with each other. (*A*2) The red and blue cells exchanged their locations. They cannot interact with their new neighbors instantaneously. Note that the red and blue cells maintain contact and interact with each other. (*A*3) and (*A*4) Interactions are gradually recovered. (*B*) Time evolution of the coupling strength defined in equation (1*b*). (*C*) Each cell experiences an exchange of its location every $1/\lambda$ time unit on average. The exchange times obey Poissonian statistics.

The vertebrate segmentation clock provides an attractive model system to address this question, because it involves intercellular signaling [6–9] together with cell movement [10–12]. This clock operates during vertebrate embryonic development and controls the rhythmic formation of somites, which are the precursors of vertebrae and other tissues that make the characteristic segmented structure of vertebrates. The segmentation clock is a tissue level rhythmic pattern generator consisting of a population of mobile cells in the presomitic mesoderm (PSM) [13, 14]. Each cell in the PSM possesses a single-cell genetic oscillator composed by negative feedback loops [15–17]. These oscillators can interact with their neighbors through membrane proteins Delta and Notch, and synchronize their phases locally [6–9].

However, by itself the local coupling through Delta–Notch signaling may be a poor way to achieve global phase synchronization across a cell population, as is observed in the tailbud, the tissue at the posterior of the PSM. The reason is that locally coupled oscillators have a strong propensity to form persistent spatial structures that prevent the cell population from reaching global synchronization [18–21]. Recently, it has been reported that cells in the posterior PSM move around and exchange their neighbors over time [10–12]. Motivated by these observations, a theoretical study suggested that cell movement observed in the posterior PSM may be important for quickly achieving global synchronization of genetic oscillators across a cell population when cells use a local coupling mechanism [21]. This result is supported by further theoretical studies addressing the effects of mobility on coupled oscillators [18, 22–24]. It has been suggested that cells moving faster synchronize their oscillators more quickly by preventing the formation of persistent spatial structures [18].

An important assumption in these previous studies is that when a cell arrives at a new location, it immediately interacts at full capacity with its new neighbors via membrane proteins (such as Delta and Notch; see [21]). However, it is reasonable to expect that the association of membrane proteins between two cells that gradually come into contact with each other might need some time to reach full capacity (figure 1(*A*), see also section 7). Indeed, such a gradual interaction was recently measured for Delta–Notch signaling in a cell culture system [25]. Here, we ask whether cellular mobility still improves synchronization when cells have to gradually recover intercellular interactions after movement.

To answer this question, we develop a coupled phase oscillator model in which we take into account both cell movement and the gradual recovery of intercellular interactions after movement. We first derive an equation for the time evolution of the coupling strength between two adjacent cells after they come into contact, by considering the kinetics of membrane protein binding events between these two cells. We use this model to show that the degree of synchronization depends in a non-monotonic way on cell movement. We find (1) an optimal moving rate for synchronization and (2) a critical moving rate above which cell movement destroys synchronization. We explain these optimal and critical moving rates in terms of the competition of timescales between the moving rate and the coupling recovery rate. Our results indicate that whether the moving rate observed *in vivo* can promote synchronization of genetic oscillators critically depends on the relative speed with which cells establish and develop interactions with their new neighbors after movement.

2. Theoretical description of mobile, coupled oscillators

We model a cell population in the tailbud as a discrete system in which cells are located on a two-dimensional lattice. The unit of length is the distance between two adjacent sites in the lattice. Each cell on the lattice is identified by the index j ($j = 1, 2, \ldots, N$). Cells in the bulk can interact with their four nearest neighbors (figure 1(*A*)), while cells in the boundaries interact with their two or three neighboring cells.

To describe the cell movement in the PSM, we allow cells on the lattice to exchange positions with one of their nearest neighbors, at random times with a characteristic time scale $1/\lambda$ (see figure 1(*C*) and section 7 for the procedures of simulations; see also [21]). The inverse of the characteristic time scale defines the moving rate λ. For larger λ, cells exchange their locations more frequently. We assume isotropic cell movement. With this representation of cell movement, a single cell performs a random walk in the lattice, as observed experimentally in the PSM [10, 11] and described in [10]. The details of movement processes, for example cell shape changes, have not been experimentally characterized in the PSM yet. Our description of cell movement is a simplification of more complex processes of movement within the tissue that allows several analytical treatments, as shown below. At the boundaries, cells exchange their positions with one of their two or three neighboring cells. This choice of boundary condition for cell movement is motivated by the fact that cells in the PSM are mostly constrained to move within the tissue.

To represent the oscillators, we adopt a locally coupled phase oscillator model [26], as was done in previous theoretical studies on the segmentation clock [21, 27, 28]. It was shown that the phase oscillator model captures the dynamics of more detailed models that explicitly describe Delta–Notch signaling for the segmentation clock [21]. Moreover, phase oscillators were successfully used to fit theory to experimental data in studies on the segmentation clock [9, 29] and the circadian clock [30, 31].

We consider the situation in which all cells have identical intrinsic frequency ω for their intracellular genetic oscillators. For the segmentation clock, this intrinsic frequency is determined by the reaction kinetics in negative feedback loops ~~in the~~ downstream of Delta–Notch signaling [16, 32]. To include the dependence of the coupling strength—the interaction rate—on the elapsed time after contact, we introduce a time-dependent coupling strength. The phase $\theta_j(t)$ of cell j at time t obeys

$$\frac{\mathrm{d}\theta_j(t)}{\mathrm{d}t} = \omega + \frac{1}{n_j}\sum_{\alpha} \kappa_{j\alpha}(t_{j\alpha}) \sin(\theta_\alpha(t) - \theta_j(t)) + \sqrt{2C}\xi_j(t) \quad \text{for} \quad j = 1, 2, \ldots, N, \tag{1a}$$

where $\sum_{a}$ represents summation over nearest neighbors, $\kappa_{j\alpha}(t_{j\alpha})$ is the time-dependent coupling strength between cell j and cell α, n_j is the number of nearest neighbors for cell j ($n_j = 2, 3$ or 4), C is the noise strength and $\xi_j(t)$ is a white Gaussian noise with $\langle \xi_j(t) \rangle = 0$ and $\langle \xi_j(t)\xi_{j'}(t') \rangle = \delta_{jj'}\delta(t - t')$. To describe the manner in which a cell takes some time to interact at full capacity with its new neighboring cells after movement (figure 1(*A*)), we introduce the following expression for coupling strength (see section 7 for a derivation of this expression where we explicitly consider simple assumptions on the kinetics of binding processes between ligands and receptors on two adjacent cells):

$$\kappa_{j\alpha}(t_{j\alpha}) = \kappa_0(1 - \mathrm{e}^{-\beta t_{j\alpha}}), \tag{1b}$$

where κ_0 is the maximum coupling strength, $t_{j\alpha}$ is the elapsed time after cell j and cell α made contact with each other, and β is the coupling recovery rate after contact. Larger β means a faster recovery of the interaction (figure 1(*B*)). The coupling strength between two adjacent cells is zero at the moment after they contact with each other. It increases with time as long as these two cells stay adjacent. To focus our analyses on this interaction-recovery process and to simplify the model, we assume that a cell that just left its position instantaneously ceases to interact with its old neighbors. The inclusion of a gradual coupling decay between old neighbors in equation (1) is an interesting extension of the model that we leave for future work.

To measure the degree of synchronization, we use the order parameter proposed by Kuramoto [33]:

$$Z(t) = \left\langle \left| \frac{1}{N}\sum_{j=1}^{N} \mathrm{e}^{\mathrm{i}\theta_j(t)} \right| \right\rangle_{\mathrm{ens}}, \tag{2}$$

where $\mathrm{i} = \sqrt{-1}$ and $\langle \cdots \rangle_{\mathrm{ens}}$ represents the average over the different realizations of initial conditions and noise (for initial conditions, see section 7). If $Z(t)$ is close to unity, the phases of oscillators are relatively close to each other and the system is in a synchronized state. In contrast, if $Z(t)$ is close to zero, phases are scattered and the system is in an unsynchronized state.

Although the order parameter equation (2) measures the degree of synchronization, it cannot characterize phase profiles that emerge in a model that includes space [18]. In order to characterize spatial phase profiles and to measure the local phase order, we also consider the correlation between two sites at distance d in the two-dimensional lattice:

$$\rho(d, t) = \langle \cos(\vartheta_{\mathbf{k}}(t) - \vartheta_{\mathbf{k}'}(t)) \rangle_{|\mathbf{k}-\mathbf{k}'|=d}, \tag{3}$$

where $\mathbf{k} = (k, l)$ represents a site in the two-dimensional lattice, $\vartheta_{\mathbf{k}}(t)$ represents the phase value of site $\mathbf{k}$ at time t (e.g. if cell j is in site $\mathbf{k}$ at time t, $\vartheta_{\mathbf{k}}(t) = \theta_j(t)$) and $\langle \cdots \rangle_{|\mathbf{k}-\mathbf{k}'|=d}$ represents an average over all pairs of sites between which the distance is d. The value of ρ lies between -1 and 1. If two sites at a distance d of each other tend to have a similar phase value, ρ is close to 1. In contrast if they tend to be opposite in phase, ρ is close to -1. If there is no correlation between them, then $\rho \approx 0$. To obtain better statistics, we calculated an average of ρ over different realizations of initial conditions and noise.

The values of parameters in the model for simulations are listed in table 1. In section 7, we estimate the moving rate λ of PSM cells as roughly around 0.05–0.1 min^{-1}, from the data in previous studies on chick somitogenesis [10, 11]. Below, we explore a wide range of the moving rate λ including these estimated values.

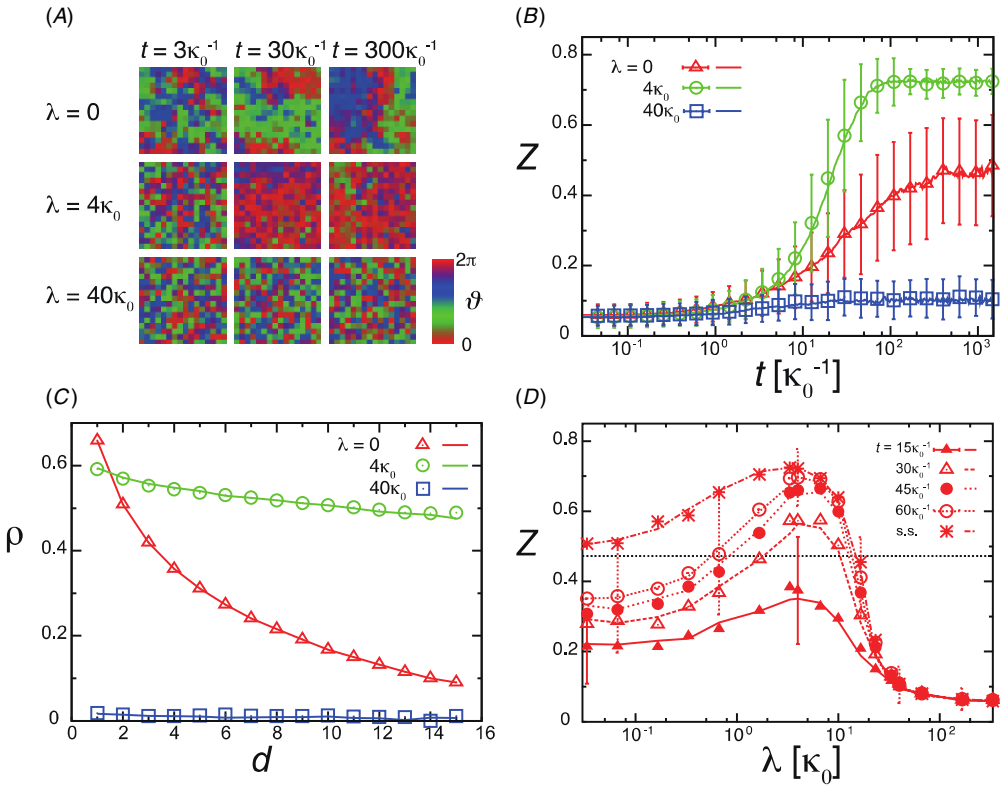

Figure 2. Dependence of the degree of synchronization on the moving rate λ is non-monotonic. (*A*) Snapshots of spatial phase profiles in the two-dimensional lattice at different moving rates λ observed in numerical simulations of equation (1*a*) with coupling recovery equation (1*b*). The phase ϑ at each site is represented by a color look-up table as indicated. (*B*)–(*D*) The symbols indicate the results of simulations of equation (1*a*) with coupling recovery equation (1*b*), while the lines indicate the results of simulations of equation (1*a*) with the effective coupling strength equation (5). (*B*) Time evolution of the order parameter $Z(t)$ defined in equation (2) at different moving rates λ as indicated. Error bars indicate standard deviations (SD). (*C*) Dependence of the correlation defined in equation (3) on the distance between two sites. We plotted the temporal average of the correlation after its value reached a steady state. Error bars for the temporal SD of correlation are smaller than the size of symbols. (*D*) Dependence of Z on the moving rate λ. Different symbols and lines correspond to different time points as indicated. 's.s.' is the steady state. The black horizontal line indicates the steady-state value of Z when $\lambda = 0$. Error bars indicate SD. In all panels, $\beta = 33\kappa_0$ and $C = 0.25\kappa_0$.

Table 1. Parameters in the model[a].

Parameters		Values used in simulations
ω	Intrinsic frequency	0
κ_0	Maximum coupling strength	0.03 min^{-1}
β	Coupling recovery rate	$3.3\kappa_0$ to $333\kappa_0$
λ	Moving rate	0 to $300\kappa_0$
C	Noise strength	$0.1\kappa_0$ to $0.3\kappa_0$
N	Number of cells in the system	256 (16 × 16)

[a]See also section 7 for these choices of parameter values.

3. Optimal and critical moving rates for synchronization

To study the effect of gradual coupling recovery, we numerically simulate equation (1) and measure the degree of synchronization by equations (2) and (3). Figures 2(*A*) and (*B*) show the snapshots of phase profiles and the time evolution of the order parameter $Z(t)$ defined in equation (2), respectively, for a fixed coupling recovery rate $\beta = 33\kappa_0$ (hereafter, we use $\kappa_0 = 0.03$ min^{-1} as the unit of time, see section 7). When cells do not move ($\lambda = 0$, red triangles in figure 2(*B*)), the order parameter increases with time and finally approaches a steady-state value around $Z = 0.5$. The standard deviations of the order parameter $Z(t)$ are large because a single trajectory of the order parameter fluctuates strongly due to noise, and the time needed for the trajectory to reach the steady-state value is sensitive to the initial phase differences (figure S1 available at stacks.iop.org/PhysScr/9/000000/mmedia). As indicated by the sharp decrease of ρ with increasing distance d in figure 2(*C*), these non-mobile cells can reach and maintain short-range correlation of phases, but they cannot achieve long-range correlation even after a long time (see also figure 2(*A*)). This means that these cells tend to form local clusters of synchronization between which phases differ greatly. When cells exchange their locations every $1/4\kappa_0$ on average ($\lambda = 4\kappa_0$, green circles in figure 2(*B*)), these cells build synchronization more rapidly compared to when they do not move. Moreover, the steady-state value of the order parameter is much larger, around $Z = 0.7$. In this case, we observe both short- and long-range correlations of phases (figures 2(*A*) and (*C*)), confirming that these cells achieve global phase order. This result is consistent with previous work using a gene network model, which shows that cell movement promotes synchronization for $\beta \gg \lambda$ (see supplementary figure S6 in [21]).

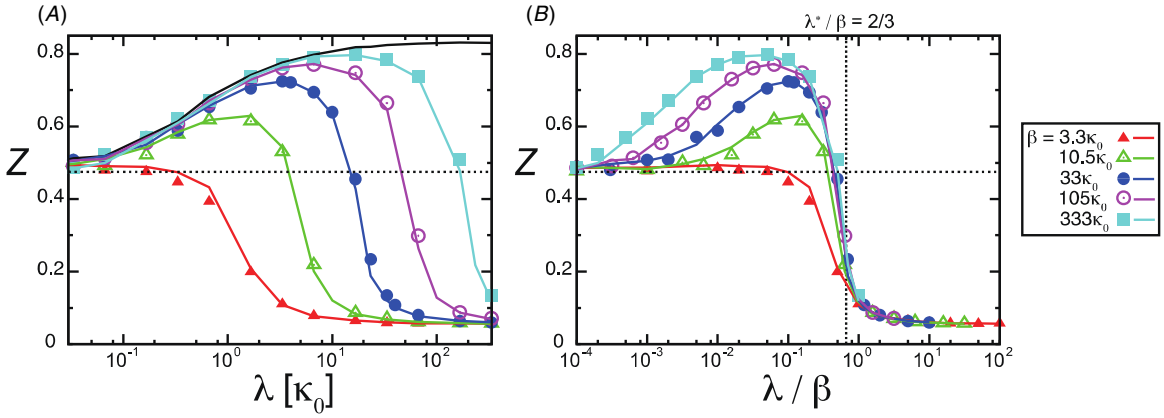

Figure 3. The optimal and critical moving rates for synchronization depend on the coupling recovery rate β. (*A*) Dependence of the order parameter Z defined in equation (2) on β at each moving rate λ. The black solid line shows the order parameter when cells can instantaneously recover interactions with their new neighbors after movement (i.e. $\kappa_{j\alpha}(t_{j\alpha})\equiv\kappa_0$ in equation (1*a*)). (*B*) Dependence of the order parameter Z defined in equation (2) on β at each ratio λ/β. The vertical dotted line indicates the transition point λ^*/β calculated from equation (8). In both panels, the symbols indicate the results of simulations of equation (1*a*) with coupling recovery equation (1*b*), while the solid lines indicate the results of simulations of equation (1*a*) with the effective coupling strength equation (5). The horizontal dotted lines in both panels indicate the steady-state value of the order parameter when $\lambda = 0$. In both panels, $C = 0.25\kappa_0$. We ran the simulations long enough for the order parameter $Z(t)$ to reach its steady-state value. We calculated the time averages of Z as described in section 7. Error bars for the temporal standard deviations of Z are smaller than the size of symbols.

However, if each cell exchanges its position more frequently than considered above ($\lambda = 40\kappa_0$, blue squares in figure 2(*B*)), the degree of synchronization is much worse than when the cells do not move ($\lambda = 0$). In this case, we observe phase-disordered states where neither local nor global phase order exists, as represented by $\rho \approx 0$ for any d in figure 2(*C*) (see also figure 2(*A*)). This indicates that the dependence of the degree of synchronization on the moving rate is non-monotonic, suggesting the existence of an optimal moving rate to achieve synchronization. We systematically studied the behavior of the order parameter for a range of moving rates, confirming the existence of an optimal moving rate (figure 2(*D*)). In addition, we found a transition point in the moving rate: if the moving rate is smaller than a critical moving rate λ^*, global phase order appears, while if it is larger than λ^* the system goes to phase disorder (figure 2(*D*), $\lambda \approx 23.3\kappa_0$). Thus, cells have to move at an appropriate rate to achieve better synchronization when they need to recover the interactions with their new neighboring cells after movement.

Both the optimal and the critical moving rates depend on the coupling recovery rate β (figure 3(*A*)). When β is small ($\beta = 3.3\kappa_0$, red filled triangles in figure 3(*A*)), no apparent peak is observable, meaning that cell movement cannot improve the degree of synchronization across the population of oscillators. In contrast, with the increase of β, an optimal moving rate for synchronization appears ($\beta = 10.5\kappa_0$–$333\kappa_0$ in figure 3(*A*)) and there is a range of the moving rate for which the degree of synchronization is better than that of non-mobile oscillators. As β increases, this range becomes wider and both the optimal and the critical moving rates become larger. These results indicate that whether cell movement at a given moving rate promotes the synchronization of oscillators depends on the coupling recovery rate. Note that the degree of synchronization achieved at each moving rate also increases with the increase in β, and eventually saturates to the value corresponding to instantaneous coupling recovery (i.e. for $\kappa_{j\alpha}(t_{j\alpha}) \equiv \kappa_0$ in equation (1*a*), the black solid line in figure 3(*A*)). For instantaneous coupling recovery, the order parameter Z monotonically increases with the increasing moving rate λ, as was previously shown in [21].

To expose the competition of timescales occurring between the moving rate λ and the coupling recovery rate β, we examine how the degree of synchronization in figure 3(*A*) scales with the ratio λ/β. The collapse of the curves is not complete, showing that the order parameter Z is not a single function of this ratio, but rather it depends on λ and β independently (figure 3(*B*)). However, the transition point from phase order to phase disorder coincides at around $\lambda/\beta = 0.7$ for large enough β. This implies that the transition point does not depend on individual values of λ and β, but on the ratio λ/β if β is large.

We next examined how noise affects optimal and critical moving rates. As the noise strength C increases, the critical moving rate becomes smaller (figure 4(*A*)). This result indicates that noise reduces the range of λ/β in which cell movement enhances the degree of synchronization. When C is small, the maximum degree of synchronization at the optimal moving rate is not very pronounced in steady states (e.g. $C = 0.1\kappa_0$ in figure 4(*A*)). However, even for small C, there is an optimal moving rate at which cells synchronize much faster than non-mobile cells (figure 2(*D*)). This optimal moving rate becomes smaller as C increases. In summary, both the coupling recovery rate β and the noise strength C determine the range in which cell movement can improve the degree of synchronization.

4. The origin of optimal and critical moving rates

To understand the optimal moving rate and to estimate the critical moving rate, we introduce an effective coupling strength. This effective coupling strength approximates the

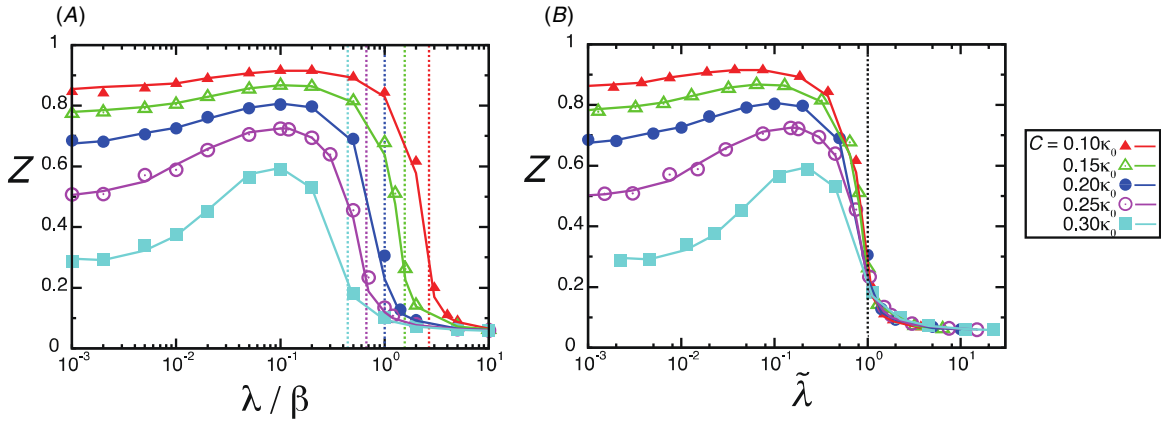

Figure 4. Noise limits the range where cell movement can improve synchronization. (*A*) The order parameter Z versus the ratio λ/β of the moving rate λ to the coupling recovery rate β for different values of the noise strength C. Each colored vertical line indicates λ^*/β calculated from equation (8) for the corresponding value of C, indicated by the line color. (*B*) Dependence of order parameter Z on the scaling parameter $\tilde{\lambda} = 3(\lambda/\beta)(\kappa_0/C - 2)$. The vertical line at $\tilde{\lambda} = 1$ indicates the transition point from phase order to phase disorder calculated from equation (8). In both panels, the symbols indicate the results of simulations of equation (1*a*) with coupling recovery equation (1*b*), while the lines indicate the results of simulations of equation (1*a*) with the effective coupling strength equation (5). In both panels, $\beta = 33\kappa_0$. We ran the simulations long enough for the order parameter $Z(t)$ to reach its steady-state value. We calculated the time averages of Z as described in section 7. Error bars for the temporal standard deviations of Z are smaller than the size of symbols.

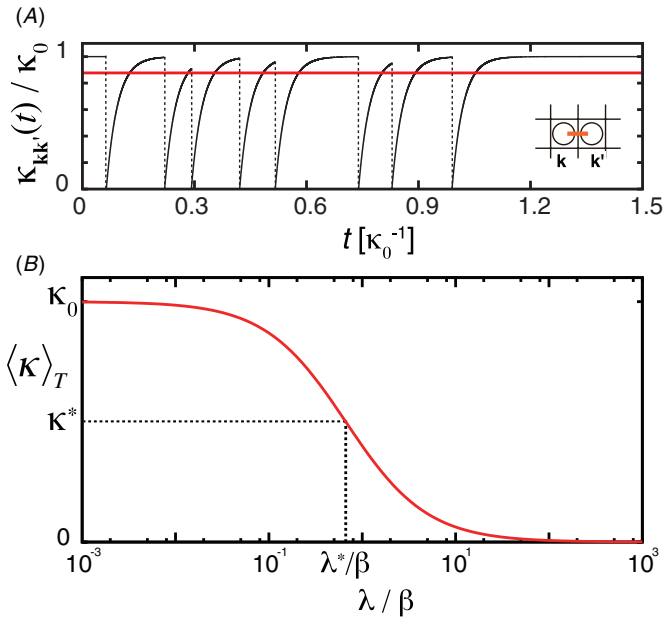

Figure 5. The effective coupling strength depends on the ratio of the moving rate to the coupling recovery rate λ/β. (*A*) Time series of the coupling strength between two adjacent sites, k and k', in a two-dimensional lattice. The red line indicates the time average of the time series. (*B*) Dependence of the time average of the coupling strength given by equation (5) on the ratio λ/β. The horizontal broken line indicates the critical coupling strength κ^* below which the disordered state is stable. The intersection between κ^* and the time average of the coupling strength determines the critical moving rate λ^*.

time-varying coupling strength between each pair of adjacent sites in the two-dimensional lattice (figure 5) by its temporal average.

Let $\kappa_{\mathbf{kk}'}(t)$ be the time series of the coupling strength between a pair of adjacent *sites* $\mathbf{k}$ and $\mathbf{k}'$ in the two-dimensional lattice (e.g. $\mathbf{k} = (k, l)$ and $\mathbf{k}' = (k, l+1)$, figures 5(*A*) and S2). As long as a pair of cells remains adjacent to each other in these two sites, $\kappa_{\mathbf{kk}'}(t)$ increases with time according to equation (1*b*). This interaction time ends when one of these two cells moves away from these two sites, and $\kappa_{\mathbf{kk}'}(t)$ is reset to zero. Note that the length of the interaction time is stochastic due to random cellular motions.

The time average of $\kappa_{\mathbf{kk}'}(t)$ between t_0 and $t_0 + T$ is defined as

$$\langle\kappa\rangle_T = \frac{1}{T}\int_{t_0}^{t_0+T} \kappa_{\mathbf{kk}'}(t)\,\mathrm{d}t, \tag{4}$$

where T is the time window for averaging. We can calculate this time average analytically by using equation (1*b*) and the probability density function for the length of the interaction time, assuming that T is sufficiently large (see the supplementary data available at stacks.iop.org/PhysScr/9/000000/mmedia for detailed calculation). The time average of the coupling strength between a pair of adjacent sites in the bulk of the two-dimensional lattice can be written as

$$\langle\kappa\rangle_T = \frac{1}{1 + 3\lambda/2\beta}\kappa_0. \tag{5}$$

Equation (5) shows that the time average of coupling strength $\langle\kappa\rangle_T$ is a decreasing function of λ/β, the ratio of the moving rate λ to the coupling recovery rate β (figure 5(*B*)). Moving faster and/or recovering the interactions slower reduces the effective coupling strength between neighboring cells. If $\lambda/\beta \ll 1$, then $\langle\kappa\rangle_T \approx \kappa_0(1 - 3\lambda/2\beta)$. In contrast, if coupling recovery is very slow and/or cells move very fast (i.e. $\lambda/\beta \gg 1$), $\langle\kappa\rangle_T \approx 2\kappa_0\beta/3\lambda$.

Equation (5) agrees with the numerically calculated time average of the coupling strength between two adjacent sites in the two-dimensional lattice (figure S2(*C*) available atstacks.iop.org/PhysScr/9/000000/mmedia for the time window $T = 300\ \kappa_0^{-1}$). Furthermore, the time evolution of the order parameter calculated from the simulations of

equation (1*a*) with $\kappa_{j\alpha}(t_{j\alpha}) \equiv \langle\kappa\rangle_T$ approximates that of the original model equation (1*a*) with equation (1*b*) very well (colored solid lines in figures 2–4).

Using equation (5), we can explain why a critical moving rate for synchronization appears (figure 5(*B*)). For coupled noisy phase oscillators, it is known that there is a critical coupling strength κ^* below which the incoherent (phase disordered) state becomes stable and global phase order is not possible [18, 34]. If the ratio λ/β is sufficiently large, $\langle\kappa\rangle_T$ becomes smaller than κ^*. Hence, cells moving faster and/or recovering interaction slower cannot achieve synchronization.

Moreover, equation (5) provides a heuristic interpretation for the dependence of the critical moving rate on the noise strength C. The noise strength C determines the critical coupling strength κ^*, and if C is large, then κ^* is also large. Therefore, the effective coupling strength $\langle\kappa\rangle_T$ becomes smaller than κ^* even at smaller λ/β. Hence, synchronization is allowed only within a reduced interval of λ/β if the noise is strong. In contrast, if the noise is weak, κ^* is smaller. Therefore, the interval in which $\langle\kappa\rangle_T$ is larger than κ^* becomes wider, allowing cells moving relatively faster to realize synchronization (figure 4).

Finally, the emergence of an optimal moving rate is explained as follows. If λ/β is sufficiently small, $\langle\kappa\rangle_T$ can be larger than κ^* (figure 5(*B*)). However, if cells move slowly enough, spatial structures that tend to hamper the achievement of global synchronization are more likely to appear (see $\lambda = 0$ in figures 2(*A*) and (*C*)). Hence, an optimal value of λ/β exists where $\langle\kappa\rangle_T$ is larger than κ^*, yet cells move fast enough to prevent the formation of persistent spatial structures (figures 3 and 5).

5. Estimation of the critical moving rate

The critical moving rate λ^* above which synchronization breaks down can be obtained from an expression for the critical coupling strength κ^*, and the expression for the effective coupling strength $\langle\kappa\rangle_T$ in equation (5) (figure 5(*B*)). Therefore, to calculate λ^*, we first need to know the critical coupling strength κ^* of mobile oscillators in a two-dimensional lattice.

Consider cells moving fast enough to meet all the cells in the two-dimensional lattice in a sufficiently short time. In such a situation, we speculate that their behavior can be approximated by that of oscillators with mean field coupling (i.e. all-to-all coupling; see[22–24]). For oscillators with mean field coupling, the critical coupling strength $\kappa_m{}^*$ below which the incoherent state is stable is

$$\kappa_m^* = 2C_m, \tag{6}$$

where C_m is the noise strength in the mean field system [34]. We approximate the critical coupling strength of mobile oscillators in a two-dimensional lattice as $\kappa^* \approx 2C$, as long as these oscillators move very fast. Therefore, the intersection between equation (5) and κ^* gives

$$\frac{1}{1+3\lambda^*/2\beta}\kappa_0 = 2C. \tag{7}$$

From equation (7), we can obtain the critical moving rate as

$$\frac{\lambda^*}{\beta} = \frac{\kappa_0/C-2}{3} \tag{8}$$

Vertical lines in figures 3(*B*) and 4(*A*) indicate λ^*/β calculated using equation (8) with the corresponding values of κ_0 and C used in simulations, showing that equation (8) is a good approximation for the transition point from phase order to phase disorder. Equation (8) further explains the scaling of the transition point among different values of β observed in figure 3(*B*) as β becomes large, for a fixed noise strength $C = 0.25\kappa_0$. Introducing the rescaled variable $\tilde{\lambda} = 3(\lambda/\beta)(\kappa_0/C-2)$, equation (8) predicts that the transition point should be at $\tilde{\lambda} = 1$. This is in fact what we see in figure 4(*B*), where the collapse of curves with different noise strengths occurs close to this transition point.

6. Discussion

In this paper, we developed a mathematical model that includes the gradual recovery of signaling between newly contacted cells after movement (figure 1) and used this model to study how this gradual recovery affects synchronization of genetic oscillators. We showed the existence of an optimal moving rate for synchronization and a critical moving rate above which synchronization is not possible (figure 2). These optimal and critical moving rates depend on the coupling recovery rate and the noise strength (figures 3 and 4). By considering the time average of the time-varying coupling strength, we derived an expression for an effective coupling strength, equation (5). This effective coupling strength reveals how the optimal and critical moving rates emerge in the system (figure 5). These interesting new properties are a direct consequence of the gradual recovery of intercellular interactions after movement and do not occur with instantaneous recovery [21]. We confirmed that our conclusions still hold even in the presence of time delays in intercellular communication [27, 29] (see supplementary data available atstacks.iop.org/PhysScr/9/000000/mmedia and figures S3 and S4). Here, to highlight the effects of the coupling recovery and make the analysis of equation (1*a*) simpler, we neglected coupling time delays.

Our results suggest that by controlling the moving rate or the recovery rate, the speed and degree of synchronization of a system can be altered experimentally. Recently, some key parameters involved in an effective theoretical description of the segmentation clock have been estimated by fitting theory to experimental data, including the coupling strength between cells, and noise strength [9, 29]. This system may offer several ways to test the effect of movement on synchronization. A naturally occurring gradient in cellular mobility has been observed along the PSM [10, 12] and different synchronization speeds may be found at different locations in the mobility gradient after experimental desynchronization. It may be possible to experimentally alter the kinetics of Delta–Notch signaling in the PSM, for example by changing the affinity of ligand and receptor [35] and thereby alter the coupling recovery rate. Moreover, a chemical factor (fibroblast growth factor) that affects the mobility of these cells has also been

identified [10, 11]. These studies suggest the possibility of regulating the ratio of the moving rate and the recovery rate experimentally and to test whether an optimal and a critical mobility exist as the current theoretical study predicts.

The finding of synchronization optima also raises the possibility that a synchronized multicellular biological clock may have evolved to an optimal ratio of the moving and recovery rate. For a system sitting in this optimal ratio, our study predicts that any perturbation to mobility or coupling recovery would be detrimental to synchronization. Furthermore, by increasing this ratio beyond the critical value, synchronization would be severely disrupted.

In other developmental processes like epiboly, gastrulation and convergence-extension, as well as in pathological situations such as inflammation and metastasis, cell movements take place at the same time as cell–cell signaling [4, 5, 36–39]. In microbial communities and in pathogen–host interactions, cell-contact signaling and movement also occur together [40]. In these processes, the type of cellular movement might differ from that observed in the PSM. However, the essential point is that cellular mobility can cause a new contact between cells that were previously distant from each other. Generally, in cellular systems intercellular communication is established and developed gradually over a characteristic time. Our study indicates that the competition between this characteristic time scale and that given by mobility is key to the ability of the system to organize spatiotemporal patterns.

7. Materials and methods

7.1. Coupling strength dynamics

To derive the coupling strength given by equation (1*b*), we consider an event in which two adjacent cells begin to interact with each other through receptors and ligands expressed on their cell surfaces. We make a few simplifying assumptions about the kinetics of binding events to obtain an expression for the resulting coupling strength. Let $p(t)$ be the amount of receptor–ligand pairs already bound at time t. The time evolution of $p(t)$ is given by the following equation:

$$\frac{\mathrm{d}p}{\mathrm{d}t} = \beta(p_\mathrm{s} - p), \tag{9}$$

where p_s is the saturating capacity (i.e. the total amount of receptor–ligand pairs available per cell–cell contact) and β is the rate of binding processes. The difference $p_\mathrm{s} - p$ is the amount of receptor–ligand pairs that have not yet bound together. In reality, p_s might change with time due to the increase or the decrease of the total amount of receptors and ligands. However, here we assume for simplicity that p_s is constant over time. With this assumption, equation (9) can be solved analytically with the initial condition $p(0) = 0$:

$$p(t)/p_\mathrm{s} = 1 - \mathrm{e}^{-\beta t}. \tag{10}$$

Assuming that the coupling strength is proportional to the ratio $p(t)/p_\mathrm{s}$ gives us equation (1*b*).

In the segmentation clock, the coupling strength κ is related to the number of available receptor molecules, Notch and ligand Delta [6–9]. Apart from the Delta–Notch signaling pathway, no other mechanism has been identified in this system to mediate intercellular coupling.

In a tissue, moving cells come into contact gradually, and consequently, their contact surface grows gradually [36]. Our model for cell movement does not include such gradual contact growth, because cells in our model just exchange their positions in a two-dimensional lattice when they move. Thus, equation (1*b*) can be interpreted as an effective description for gradual contact growth in the context of a lattice model.

7.2. The integration scheme for equation (1)

In this paper, we use a two-dimensional square lattice. Cells in the lattice exchange positions with their neighbors at random times. We assume that the probability that each cell changes its location per unit time is λ. The time interval until the next exchange event occurs is determined using the Gillespie algorithm [41]. Equation (1) is then integrated with the Heun method between two successive exchange events. The time step Δt_s for numerical integration is fixed during a single simulation, and is determined such that for a given value of the moving rate λ, Δt_s is smaller than the average time interval until the next exchange event $1/(\lambda N/2)$, as $10\Delta t_s \approx 1/(\lambda N/2)$. If $\Delta t_s > 0.01$ in this equation, we set $\Delta t_s = 0.01$. In the simulations, when a time interval until the next exchange event given by the Gillespie algorithm is smaller than Δt_s, we accept this exchange event at the next time point.

7.3. Parameter values

Throughout this paper, we fix $\omega = 0$ without loss of generality, considering the system from a co-rotating reference frame. We use $\kappa_0 = 0.03\ \mathrm{min}^{-1}$, which is based on estimations of the coupling strength in vertebrate somitogenesis obtained from theory fits to experimental data [9, 29]. However, our results are not qualitatively sensitive to the value of κ_0. Similarly, we take a typical size of the relevant tissue during somitogenesis, a square lattice of 16×16, with a total of $N = 256$ cells [21]. As the domain size becomes larger, oscillators need more time to achieve synchronization (figure S5 available at stacks.iop.org/PhysScr/9/000000/mmedia). In addition, a steady-state value of the order parameter Z is smaller for a larger domain size than for a smaller one. However, for different domain sizes, our main results are qualitatively the same (figure S5 available at stacks.iop.org/PhysScr/9/000000/mmedia). The choice of boundary conditions does not affect our conclusions either (figure S6 available at stacks.iop.org/PhysScr/9/000000/mmedia).

Recent measurements of cellular mobility in the posterior chick PSM [10, 11] provided values of cellular velocity of about 0.5–1.0 μm min^{-1}. Assuming the average cell diameter of 10 μm, these data suggest that cells move about one cell diameter roughly in 10–20 min, which gives the moving rate of 0.05–0.1 min^{-1}. This observed cell movement seems rapid enough compared to the period of the chick segmentation clock, which is around 90 min [42]. In fact, a previous study demonstrated that cell movement at the above estimated rates can improve synchronization even under an oscillatory period of 30 min in simulations [21].

7.4. Initial conditions

The initial phase of each oscillator is chosen randomly from a uniform distribution between 0 and 2π. In this paper, the order parameter equation (2) and the correlation equation (3) are calculated from 200 realizations of the initial conditions and noise unless otherwise indicated. At the initial time, the coupling strength for each pair of adjacent cells is set to its maximum capacity κ_0. If a cell contacts with new cells after movement in the simulations, the coupling strength between them changes according to equation (1*b*).

7.5. Steady-state measurements

The simulations are run long enough for the order parameter defined in equation (2) and the correlation defined in equation (3) to reach steady-state values (figure S7 available at stacks.iop.org/PhysScr/9/000000/mmedia). The time taken to reach steady-state values strongly depends on the moving rate λ. For this reason, we use different calculation times, ranging from 150 ${\kappa_0}^{-1}$ to 1500 ${\kappa_0}^{-1}$ depending on the value of λ, to optimize computational costs. The steady-state measurement we report in figures 2–4 is the temporal average of the order parameter and the correlation calculated using the last 90 ${\kappa_0}^{-1}$ time span.

Acknowledgments

We thank the group of Professor Jülicher and the Max Planck Institute for the Physics of Complex Systems for their hospitality and insightful discussions. KU is supported by the Japan Society for the Promotion of Science for Young Scientists. SA acknowledges grant MOSAICO (Ministerio de Ciencia e Innovación, Spain). LGM acknowledges CONICET and ANPCyT PICT 876. ACO and LGM are supported by the Max Planck Society and by the European Research Council under the European Communities 7th Framework Programme (FP7/2007–2013) / ERC grant number 207634.

References

[1] Andersson E R, Sandberg R and Lendahl U 2011 Notch signaling: simplicity in design, versatility in function *Development* **138** 3593–612
[2] Pitulescu M E and Adams R H 2010 Eph/ephrin molecules—a hub for signaling and endocytosis *Genes Dev.* **24** 2480–92
[3] Stepniak E, Radice G L and Vasioukhin V 2009 Adhesive and signaling functions of cadherins and catenins in vertebrate development *Cold Spring Harb. Perspect. Biol.* **1** a002949
[4] Friedl P and Gilmour D 2009 Collective cell migration in morphogenesis, regeneration and cancer *Nature Rev. Mol. Cell Biol.* **10** 445–57
[5] Solnica-Krezel L 2005 Conserved patterns of cell movements during vertebrate gastrulation *Curr. Biol.* **15** R213–28
[6] Horikawa K, Ishimatsu K, Yoshimoto E, Kondo S and Takeda H 2006 Noise-resistant and synchronized oscillation of the segmentation clock *Nature* **441** 719–23
[7] Jiang Y J, Aerne B L, Smithers L, Haddon C, Ish-Horowicz D and Lewis J 2000 Notch signalling and the synchronization of the somite segmentation clock *Nature* **408** 475–9
[8] Ozbudak E M and Lewis J 2008 Notch signalling synchronizes the zebrafish segmentation clock but is not needed to create somite boundaries *PLoS Genet.* **4** e15
[9] Riedel-Kruse I H, Muller C and Oates A C 2007 Synchrony dynamics during initiation, failure, and rescue of the segmentation clock *Science* **317** 1911–5
[10] Benazeraf B, Francois P, Baker R E, Denans N, Little C D and Pourquie O 2010 A random cell motility gradient downstream of FGF controls elongation of an amniote embryo *Nature* **466** 248–52
[11] Delfini M C, Dubrulle J, Malapert P, Chal J and Pourquie O 2005 Control of the segmentation process by graded MAPK/ERK activation in the chick embryo *Proc. Natl Acad. Sci. USA* **102** 11343–8
[12] Mara A, Schroeder J, Chalouni C and Holley S A 2007 Priming, initiation and synchronization of the segmentation clock by deltaD and deltaC *Nature Cell Biol.* **9** 523–30
[13] Oates A C, Morelli L G and Ares S 2012 Patterning embryos with oscillations: structure, function and dynamics of the vertebrate segmentation clock *Development* **139** 625–39
[14] Pourquie O 2011 Vertebrate segmentation: from cyclic gene networks to scoliosis *Cell* **145** 650–63
[15] Hirata H, Yoshiura S, Ohtsuka T, Bessho Y, Harada T, Yoshikawa K and Kageyama R 2002 Oscillatory expression of the bHLH factor Hes1 regulated by a negative feedback loop *Science* **298** 840–3
[16] Lewis J 2003 Autoinhibition with transcriptional delay: a simple mechanism for the zebrafish somitogenesis oscillator *Curr. Biol.* **13** 1398–408
[17] Oates A C and Ho R K 2002 Hairy/E(spl)-related (Her) genes are central components of the segmentation oscillator and display redundancy with the Delta/Notch signaling pathway in the formation of anterior segmental boundaries in the zebrafish *Development* **129** 2929–46
[18] Peruani F, Nicola E M and Morelli L G 2010 Mobility induces global synchronization of oscillators in periodic extended systems *New J. Phys.* **12** 093029
[19] Tiedemann H B, Schneltzer E, Zeiser S, Rubio-Aliaga I, Wurst W, Beckers J, Przemeck G K H and De Angelis M H 2007 Cell-based simulation of dynamic expression patterns in the presomitic mesoderm *J. Theor. Biol.* **248** 120–9
[20] Tinsley M R, Taylor A F, Huang Z Y and Showalter K 2009 Emergence of collective behavior in groups of excitable catalyst-loaded particles: spatiotemporal dynamical quorum sensing *Phys. Rev. Lett.* **102** 158301
[21] Uriu K, Morishita Y and Iwasa Y 2010 Random cell movement promotes synchronization of the segmentation clock *Proc. Natl Acad. Sci. USA* **107** 4979–84
[22] Frasca M, Buscarino A, Rizzo A, Fortuna L and Boccaletti S 2008 Synchronization of moving chaotic agents *Phys. Rev. Lett.* **100** 044102
[23] Fujiwara N, Kurths J and Diaz-Guilera A 2011 Synchronization in networks of mobile oscillators *Phys. Rev.* E **83** 025101
[24] Skufca J D and Bollt E M 2004 Communication and synchronization in disconnected networks with dynamic topology: moving neighborhood networks *Math. Biosci. Eng.* **1** 347–59
[25] Sprinzak D, Lakhanpal A, Lebon L, Santat L A, Fontes M E, Anderson G A, Garcia-Ojalvo J and Elowitz M B 2010 Cis-interactions between Notch and Delta generate mutually exclusive signalling states *Nature* **465** 86–90
[26] Sakaguchi H, Shinomoto S and Kuramoto Y 1987 Local and global self-entrainments in oscillator lattices *Prog. Theor. Phys.* **77** 1005–10
[27] Morelli L G, Ares S, Herrgen L, Schroter C, Julicher F and Oates A C 2009 Delayed coupling theory of vertebrate segmentation *HFSP J.* **3** 55–66

[28] Murray P J, Maini P K and Baker R E 2011 The clock and wavefront model revisited *J. Theor. Biol.* **283** 227–38
[29] Herrgen L, Ares S, Morelli L G, Schroter C, Julicher F and Oates A C 2010 Intercellular coupling regulates the period of the segmentation clock *Curr. Biol.* **20** 1244–53
[30] Liu C, Weaver D R, Strogatz S H and Reppert S M 1997 Cellular construction of a circadian clock: period determination in the suprachiasmatic nuclei *Cell* **91** 855–60
[31] Yang Q, Pando B F, Dong G G, Golden S S and Van Oudenaarden A 2010 Circadian gating of the cell cycle revealed in single cyanobacterial cells *Science* **327** 1522–6
[32] Uriu K, Morishita Y and Iwasa Y 2009 Traveling wave formation in vertebrate segmentation *J. Theor. Biol.* **257** 385–96
[33] Kuramoto Y 1984 *Chemical Oscillations, Waves and Turbulence* (Berlin: Springer)
[34] Strogatz S H and Mirollo R E 1991 Stability of incoherence in a population of coupled oscillators *J. Stat. Phys.* **63** 613–35
[35] Cordle J, Redfield C, Stacey M, Van Der Merwe P A, Willis A C, Champion B R, Hambleton S and Handford P A 2008 Localization of the delta-like-1-binding site in human notch-1 and its modulation by calcium affinity *J. Biol. Chem.* **283** 11785–93
[36] Bertet C, Sulak L and Lecuit T 2004 Myosin-dependent junction remodelling controls planar cell intercalation and axis elongation *Nature* **429** 667–71
[37] Keller R 2002 Shaping the vertebrate body plan by polarized embryonic cell movements *Science* **298** 1950–4
[38] Rorth P 2011 Whence directionality: guidance mechanisms in solitary and collective cell migration *Dev. Cell* **20** 9–18
[39] Wallingford J B, Fraser S E and Harland R M 2002 Convergent extension: the molecular control of polarized cell movement during embryonic development *Dev. Cell* **2** 695–706
[40] Bassler B L and Losick R 2006 Bacterially speaking *Cell* **125** 237–46
[41] Gillespie D T 1977 Exact stochastic simulation of coupled chemical-reactions *J. Phys. Chem.* **81** 2340–61
[42] Palmeirim I, Henrique D, Ish-Horowicz D and Pourquie O 1997 Avian hairy gene expression identifies a molecular clock linked to vertebrate segmentation and somitogenesis *Cell* **91** 639–48

QUERIES

Page 1
Q1
Author: Please be aware that the color figures in this article will only appear in color in the Web version. If you require color in the printed journal and have not previously arranged it, please contact the Production Editor now.

Page 9
Q2
Author: Please check the details for any journal references that do not have a blue link as they may contain some incorrect information. Pale purple links are used for references to arXiv e-prints.